

Contents lists available at ScienceDirect

Advanced Powder Technology

journal homepage: www.elsevier.com/locate/apt

Original Research Paper

Removal of methyl orange by multiwall carbon nanotube accelerated by ultrasound devise: Optimized experimental design

M. Ghaedi ^{a,*}, S. Hajati ^b, M. Zaree ^a, Y. Shajaripour ^a, A. Asfaram ^a, M.K. Purkait ^c^a Chemistry Department, Yasouj University, Yasouj 75918-74831, Iran^b Physic Department, Yasouj University, Yasouj 75918-74831, Iran^c Department of Chemical Engineering, Indian Institute of Technology Guwahati, Guwahati 781039, Assam, India

ARTICLE INFO

Article history:

Received 24 October 2014

Received in revised form 13 April 2015

Accepted 2 May 2015

Available online xxxx

Keywords:

Adsorption

Central composite design

Methyl orange (MO)

Multiwalled carbon nanotubes

Ultrasound assisted removal

ABSTRACT

This study investigates the methyl orange (MO) removal from aqueous solution through the application of ultrasound onto multiwalled carbon nanotubes (MWCNTs). Characterization of MWCNT was carried out using scanning electron microscopy (SEM) and tunneling electron microscopy (TEM). The influences of various parameters on the removal percentage were studied and optimized by a central composite design (CCD) and response surface methodology (RSM). Results indicate that a small amount of proposed adsorbent (0.025 g) is responsible for successful removal of 15 mg L⁻¹ of MO (RE > 99%) in a short time (3.4 min) and pH of 1–2. Adsorption kinetic data are fitted well with pseudo second order model. Equilibrium data followed Langmuir isotherm model with maximum adsorption capacity of 53.76 mg g⁻¹.

© 2015 The Society of Powder Technology Japan. Published by Elsevier B.V. and The Society of Powder Technology Japan. All rights reserved.

1. Introduction

Dyes with adverse effects on human body [1] applied in textile, dyeing, printing, and related industries led to large amounts of dye-containing wastewater and their subsequent discharge into environment associated with generation of hazards for human health [2,3]. Methyl orange (MO, a water-soluble azo dye in addition to above activities widely used in research laboratories as an acid base indicator [4]. This dye is entering the body through ingestion metabolizes into aromatic amines by intestinal microorganisms. Liver reductive enzymes catalyze the reductive cleavage of the azo linkage to produce aromatic amines and generation of cancer [5,6]. Therefore, the MO removal before discharging to environment is necessary and accomplished via photocatalytic degradation [7], advanced oxidation [8], electrochemical oxidation [9], ultrafiltration [10] and adsorption [11–13]. Adsorption process due to remarks viz. simplicity in operation, high adsorption capacity is good applicable approaches for dye removal from various systems [14–16]. Application of MWCNT cause achievement of high adsorption capacity and fast removal using small amount of adsorbent in short time [17,18]. Ultrasound irradiation accelerate the rate of chemical process by formation of acoustic cavitations that

facilitate mass transfer following propagation of pressure wave through liquid [19,20]. The ultrasound radiation led to increase in rate of mass transfer through migration and diffusion [21,22]. Optimization based experimental design help the researchers to ascertain interactions among the operating variables for the simultaneous optimization and investigation of the effects of variables with least number of experiments [23,24].

From the above literatures it is envisaged that the use of multi-wall carbon nanotube as an adsorbent for the removal of Methyl orange dye has not been investigated. Present work explored the possibility of MWCNT application as an adsorbent for MO removal from aqueous medium. The adsorption performance was enhanced by applying sonication. Influence of important variables (pH, amount of adsorbent, initial MO concentration and contact time) were investigated and optimized by central composite design (CCD) combined with response surface methodology (RSM). The proposed technique might be of useful and cost effectives for quantitative adsorption of MO as effective adsorbent.

2. Experimental

2.1. Instruments and reagents

The methyl orange (Fig. 1) dye concentration was determined using Jusco UV-visible spectrophotometer model V-530 (Jasco, Japan) at a wavelength of 473 nm while the pH/ion meter

* Corresponding author. Tel./fax: +98 741 2223048.

E-mail addresses: m_ghaedi@yu.ac.ir, m_ghaedi@mail.yu.ac.ir, m_ghaedi@yahoo.com (M. Ghaedi).

<http://dx.doi.org/10.1016/j.apt.2015.05.002>

0921-8831/© 2015 The Society of Powder Technology Japan. Published by Elsevier B.V. and The Society of Powder Technology Japan. All rights reserved.

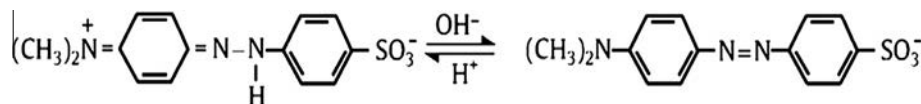


Fig. 1. Chemical structure of MO.

(Metrohm, model-686, Switzerland, Swiss) was used for the measurement of pH of solution. The morphology of the multiwalled carbon nanotube (MWCNT) was observed by scanning electron microscopy (SEM; Hitachi S-4160, Tokyo, Japan) under an acceleration voltage of 15 kV. The morphology and the size distribution of the MWCNTs were determined by a Hitachi H-800 TEM (Hitachi, Japan) at an operating voltage of 200 kV. An ultrasonic bath with heating system (Techno-GAZ SPA Ultra Sonic System, Bologna, Italy) at frequency 40 kHz and power 130 W was used for the ultrasound-assisted adsorption procedure. All chemicals including NaOH, HCl, KCl and methyl orange (MO) with the highest purity available were purchased from Merck (Dermasdat, Germany). The stock MO solution was prepared by dissolving appropriate amount of solid dye in double distilled water and the desired concentrations of test solutions were prepared by diluting the stock solution. X-ray diffraction (XRD) pattern was recorded by an automated Philips X'Pert X-ray diffractometer with Cu K α radiation (40 kV and 30 mA) for 2θ values over 10–90°. Fourier transform infrared spectroscopy (FTIR in the range of 400–4000 cm^{-1}) of the adsorbent was recorded using FTIR spectrophotometer (Model: FT-IR JASCO 460 Plus). The spectra obtained were analyzed.

2.2. Ultrasound assisted adsorption method

The MO removal experiments were performed under ultrasound using MWCNT as adsorbent. The sonochemical adsorption experiment was carried out in batch mode as follows: specified amounts of MO dye solution at known concentration (15 mg L^{-1}) and initial pH of 1 with a known amount of adsorbent (0.025 g) were poured into the flask and maintained the desired sonication time (3.4 min). At the end of the adsorption experiments, the sample was immediately centrifuged and analyzed. Details of experimental procedure and calculation are reported in our earlier work [3].

2.3. Multiwalled carbon nanotubes

Multiwalled carbon nanotubes (MWCNT) were purchased from Merck. The purity of the as-received MWCNTs material was >95% and its outside and inside diameters were 10–20 nm and 5–10 nm, respectively. The length of these MWCNT was 10–30 μm . These specification details were given by the manufacturer. The surface area (BET) of MWCNT was measured around 200 $\text{m}^2 \text{g}^{-1}$.

2.4. Central composite design (CCD)

The CCD was used to investigate the significance of the effects of parameters including pH, amount of adsorbent, initial MO concentration and contact time. A five-level CCD was performed to evaluate the variables influence (sole and interaction) on removal percentage (Table 1) that leads to 31 runs for the optimization process. Table 2 shows the experimental design points consists of 2^n factorial points with $2n$ axial points ($\alpha = 2$ distance from center), N_c central points (to estimate experimental error and the reproducibility of the data) and the test results for the response variables. The mathematical relationship between the

Table 1
Experimental factors and levels in the central composite design.

Factors	Levels			Star point $\alpha = 2$	
	Low (-1)	Central (0)	High (+1)	$-\alpha$	$+\alpha$
(X ₁) pH	2.5	4.0	5.5	1.1	7.0
(X ₂) Adsorbent dosage (g)	0.015	0.025	0.035	0.005	0.045
(X ₃) MO concentration (mg L^{-1})	10	15	20	5	25
(X ₄) Contact time (min)	2.0	35	5.0	0.5	6.5

Table 2
Data statistics of model variables.

Runs	X ₁	X ₂	X ₃	X ₄	Removal (%)
29	4.0	0.025	15	3.5	73.39
13	2.5	0.015	20	5.0	77.19
24	4.0	0.025	15	6.5	69.10
6	5.5	0.015	20	2.0	63.26
16	5.5	0.035	20	5.0	70.27
19	4.0	0.005	15	3.5	40.73
12	5.5	0.035	10	5.0	64.86
26	4.0	0.025	15	3.5	83.02
14	5.5	0.015	20	5.0	59.10
4	5.5	0.035	10	2.0	65.75
20	4.0	0.045	15	3.5	85.99
8	5.5	0.035	20	2.0	80.79
30	4.0	0.025	15	3.5	82.73
15	2.5	0.035	20	5.0	91.18
2	5.5	0.015	10	2.0	69.86
3	2.5	0.035	10	2.0	98.13
31	4.0	0.025	15	3.5	76.85
22	4.0	0.025	25	3.5	73.12
10	5.5	0.015	10	5.0	67.12
5	2.5	0.015	20	2.0	60.29
28	4.0	0.025	15	3.5	76.78
9	2.5	0.015	10	5.0	97.24
27	4.0	0.025	15	3.5	79.46
21	4.0	0.025	5	3.5	82.17
18	7.0	0.025	15	3.5	64.60
1	2.5	0.015	10	2.0	87.50
11	2.5	0.035	10	5.0	99.17
25	4.0	0.025	15	3.5	75.89
7	2.5	0.035	20	2.0	88.24
23	4.0	0.025	15	0.5	66.96
17	1.0	0.025	15	3.5	91.75

four independent variables was approximated by the second order polynomial model [25,26].

Response surface methodology (RSM) allows the determination and evaluation of the relative significance of parameters on the process. The modeling was performed to estimate first or second order polynomials equations following analysis of variances (ANOVA). Results were plotted in tridimensional graph and allow surface response corresponds to a response function that always used for prediction of real optimum points.

3. Results and discussion

3.1. Characterization of MWCNTs

The Field Emission Scanning Electron Microscopy (FESEM) image of the MWCNTs is shown in Fig. 2(a). It can be seen that

the surface morphology of the MWCNTs is homogeneous and smooth. The Transmission electron microscopy (TEM) image of the MWCNT is outlined in Fig. 2(b). It is clear from the TEM image that the MWCNTs is tube like in shape. The outside and inside diameters were measured in the range of 10–20 nm and 5–10 nm, respectively. The length of these MWCNTs was between 10 and 30 μm.

IR spectrum of MWCNT shows some important characteristic vibrational frequencies at 3415 and 1573 (Fig. 3(a)). IR spectrum of MWCNTs shows some characteristic frequencies at 3415 and 1573 cm⁻¹ which are attributed to O–H phenolic, RNH₂ stretching NH₂ in plane bend.

Raman studies of MWCNTs with large diameter distribution indicated quite strong similarities to the well-known SWCNT modes. In the Raman spectrum of MWCNTs two sharp Raman peaks are seen. The G band which assigned to the in-plane vibration of the C–C bond (defective graphite-like in-plane mode) and the D band (a disorder in carbon systems) appear at about 1580 cm⁻¹, and about 1340 cm⁻¹, respectively.

3.2. Central composite design (CCD)

The CCD step (Tables 1 and 2) was used to estimate the main and interaction of variables (pH (x_1), adsorbent dosage (x_2), MO concentration (x_3) and contact time (x_4)) in three levels (low, basal and high) with coded value (-1, 0, +1) and the star points of +2 and -2 for + α and - α , respectively (31 experiments). Application of analysis of variance (ANOVA) (Table 3) give useful information about significance of all variables and their interaction based on *F*-test and considering *p*-value at 95% confidence level. Data analysis gave a semi-empirical expression of removal percentage (R%) with following equation:

$$y = 78.3 - 17.8x_1 + 14.01x_2 - 6.52x_3 - 11.113x_2^2 + 17.95x_1x_3 + 15.9x_2x_4 \quad (1)$$

3.3. Response surface methodology (RSM)

RSM application following CCD possible to achieve optimization of the critical factors and give useful information about the response nature. Fig. 3 represents the relevant fitted response surfaces for the design and depicts the response surface plots of removal (%) versus variables. The curvature nature of plots confirms the presence of interaction among variables. The response surfaces plots (Fig. 3a) indicate dependency of removal percentage

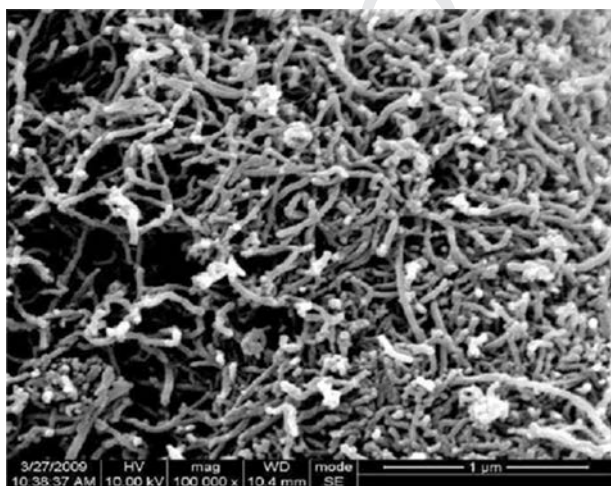


Fig. 2. (a) SEM image of the MWCNTs and (b) typical TEM image of the MWCNTs.

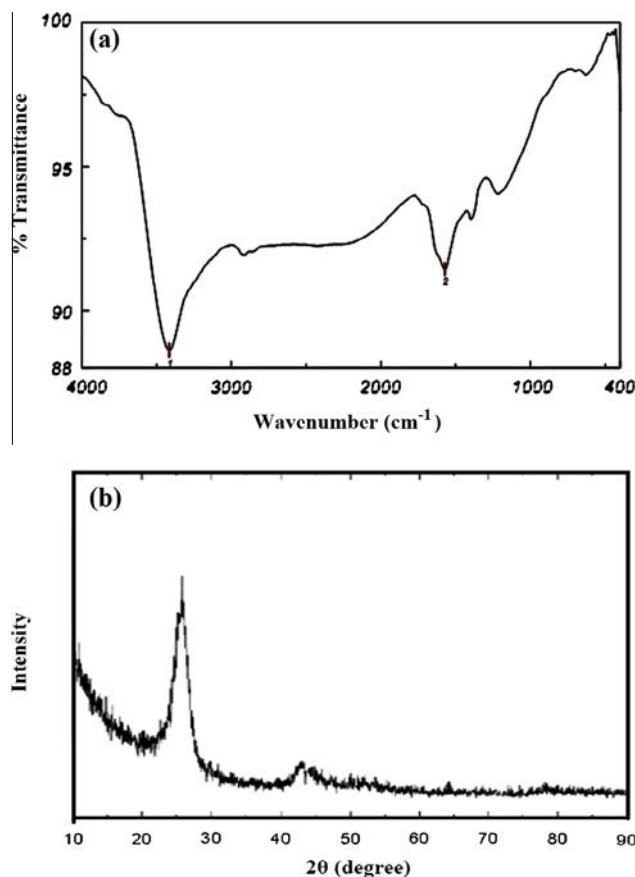


Fig. 3. Response surfaces for the CCD.

Table 3
Analysis of variance (ANOVA) for CCD.

Source of variation	Sum of square	Df	Mean square	F-value	P-value
X_1	1876.732	1	1876.732	145.1494	0.000020
X_1^2	24.051	1	24.051	1.8601	0.221556
X_2	1166.918	1	1166.918	90.2512	0.000078
X_2^2	222.058	1	222.058	17.1743	0.006050
X_3	249.680	1	249.680	19.3106	0.004596
X_3^2	17.603	1	17.603	1.3615	0.287555
X_4	11.468	1	11.468	0.8869	0.382663
X_4^2	74.968	1	74.968	5.7982	0.052722
X_1X_2	64.682	1	64.682	5.0026	0.066654
X_1X_3	314.796	1	314.796	24.3468	0.002619
X_1X_4	149.634	1	149.634	11.5729	0.014462
X_2X_3	259.613	1	259.613	20.0789	0.004188
X_2X_4	46.138	1	46.138	3.5684	0.107799
X_3X_4	0.248	1	0.248	0.0191	0.894485
Lack-of-fit	521.071	10	52.107	4.0300	0.050838
Pure error	77.578	6	12.930		
Total	5098.686	30			

to variables such as adsorbent dosage, pH, MO concentration and contact time. The removal percentage has positive and similar trend with adsorbent mass, while the higher removal percentage at higher adsorbent mass is attributed to its high specific surface area. Significant decrease in the removal percentage at lower amount of adsorbent was observed due to possible saturation of reaction sites. Fig. 3b confirms the rapid adsorption of MO that support strong requirement of ultrasound power to accelerate mass transfer. The initial fast adsorption is attributed to increase in available surface area and vacant site following efficient

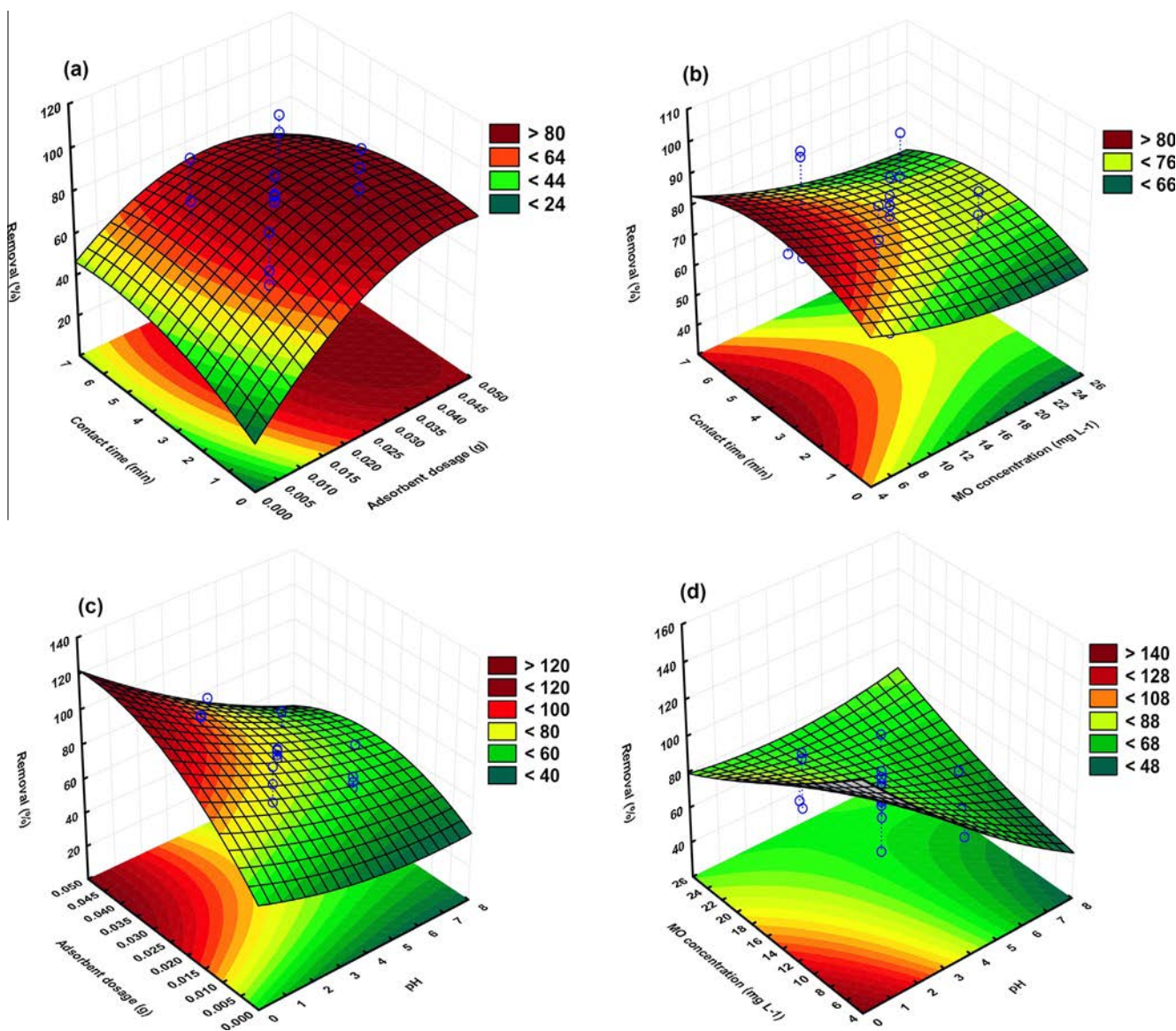


Fig. 4. Profiles for predicted values for removal percentage of MO.

dispersion of adsorbent into solution by ultrasonic irradiations, which simultaneously increase the dye diffusion coefficient and the surface atoms and area of adsorbent. The increase in MO removal percentage with decrease in pH is accredited to increase in reaction sites at this region (Fig. 3c). At low initial pH, MWCNTs due to the protonation get positive charge and strong attractive forces among the MO (anionic dye) and MWCNT lead to improve in removal percentage. At high pH, MWCNT functional group completely deprotonated and get negative charge and via electrostatic repulsive force hinder from further adsorption. On the other hand, the dye molecules also get negatively charged and/or even due to presence of OH group, increase the repulsive force between dyes and adsorbent. The effect of initial MO concentration on its removal percentage (Fig. 3d) shows that the amount of dye uptake and removal efficiency has opposite direction and decrease in removal percentage at higher initial dye concentration was seen.

The Mo removal is a fast process and more than 80% was occurred in the first 4 min and reach equilibrium at about 7 min sonication time. It seems that ultrasonic irradiations simultaneously increase the MO diffusion coefficient for transfer to the

external surface reactive atoms and also lead to enhance in contact interface among MO and MWCNT. The low Mo removal percentage at the optimum conditions in the absence of ultrasonic (67%) strongly enhanced to 98.6% following exposure to the ultrasonic power. This result that expected and positive change in the adsorbent structure and/or increase in mass transfer significantly reduce at similar condition in the absence of ultrasonic.

3.4. Optimization of parameters

The profile for predicted values is used for the optimization process (Fig. 4). The overall response obtained from these plots with the current level of each variable in the model is depicted at the bottom of Fig. 4. On the basis of these calculations, maximum recovery (99.2%) was obtained at optimum conditions set as: 3.4 min of contact time, 0.025 g of adsorbent dose, initial MO concentration of 15 mg L⁻¹ and pH = 1 (see Fig. 5).

Similar experiments were undertaken at fixed same value of oxidized, non-oxidized and raw-MWCNT and it was found that the removal percentage was 97.8, 96.7, and 98.2 at contact time of 6 min. Since oxidation of MWCNT is a time

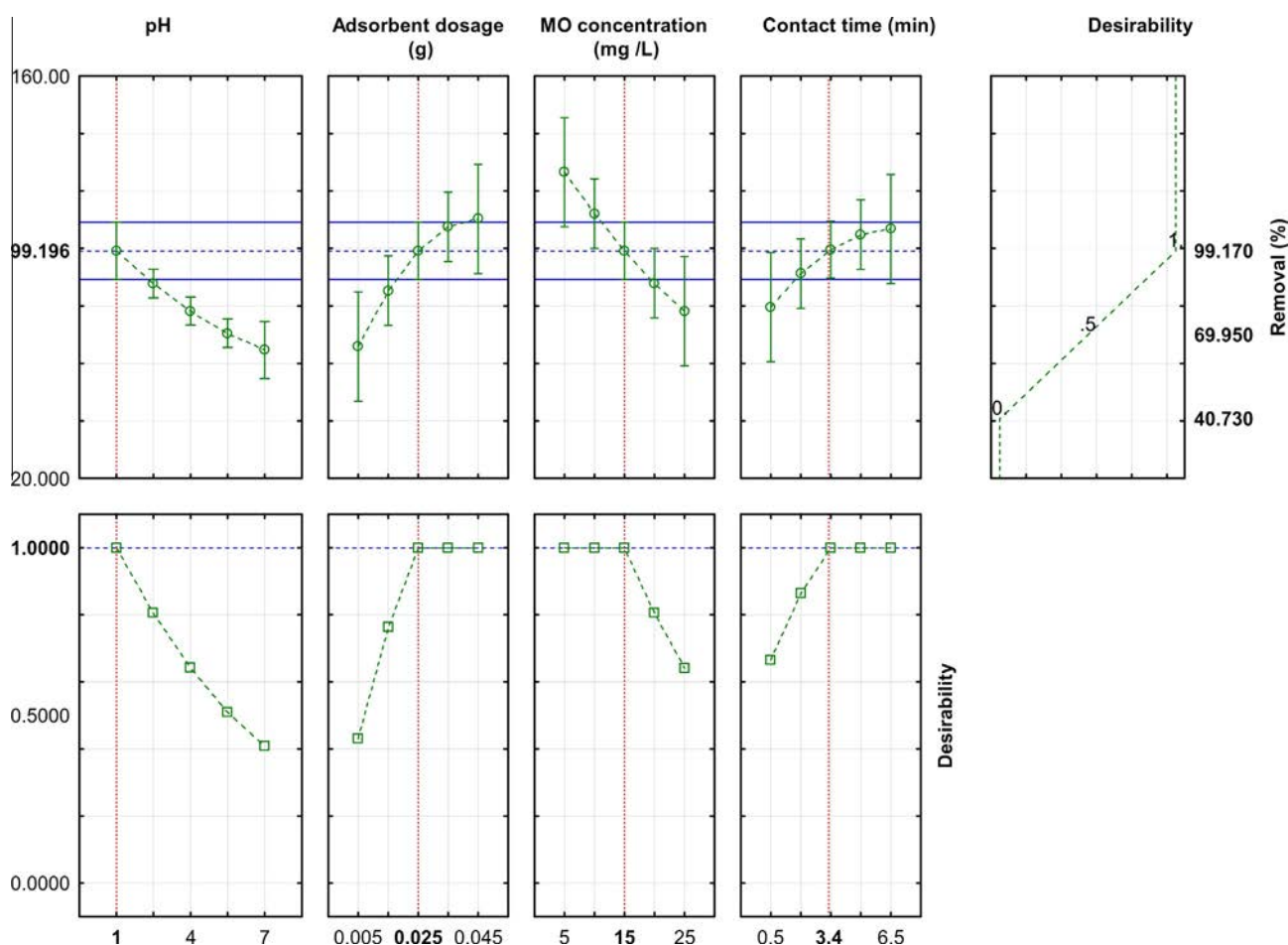


Fig. 5. Optimum value of all variables based on DF.

Table 4
Isotherm constant parameters and correlation coefficients calculated for the adsorption of MO onto MWCNTs.

Isotherm	Equation	Parameters	Value of parameters		
Langmuir	$C_e/q_e = 1/K_a Q_m + C_e/Q_m$	Q_m (mg g ⁻¹)	0.015 g	0.027 g	0.035 g
		K_a (L m g ⁻¹)	32.57	46.95	53.76
		R^2	0.405	0.699	2.120
			0.990	0.997	0.993
Freundlich	$\ln q_e = \ln K_f + (1/n)\ln C_e$	$1/n$	0.175	0.180	0.180
		K_f (L m g ⁻¹)	16.83	28.42	34.71
		R^2	0.952	0.902	0.931
Temkin	$q_e = \beta \ln k_t + \beta \ln C_e$	B_1	4.264	5.936	6.497
		K_T (L m g ⁻¹)	39.65	137.0	270.4
		R^2	0.922	0.949	0.958

consuming stage (36 h in nitric and hydrochloric acid), authors preferred to use raw-MWCNT.

3.5. Adsorption equilibrium study

Equilibrium adsorption isotherm study help the researchers to predict nature of adsorption and give useful information about the actual amount of adsorbed dyes [27]. The data obtained during equilibrium study was fitted to various adsorption equations such as Langmuir, Freundlich and Temkin isotherms to ascertain the equilibrium characteristics of the adsorption process [28–31]. Adsorption isotherms for each model obtained from the plots of known equations at initial dye concentration (5–50 mg L⁻¹), fixed amount of adsorbent (0.015, 0.027 and 0.035 g) and pH = 1

(Table 4). Based on the linear form of Langmuir isotherm model (according to Table 4), the values of K_L (the Langmuir adsorption constant (L m g⁻¹)) and Q_m (maximum adsorption capacity (mg g⁻¹)) were obtained from the intercept and slope of line by plotting C_e/q_e vs C_e , respectively. The high correlation coefficients (0.989, 0.993 and 0.996) show the applicability of Langmuir model for interpretation of the experimental data with maximum adsorption capacity of 53.76 mg g⁻¹. The parameters of Freundlich isotherm model such as K_F ((mg/g)/(mg/L)^{1/n}) and n (the capacity and intensity of the adsorption) were calculated from the intercept and slope of the linear plot of $\ln q_e$ versus $\ln C_e$, respectively (Table 4). The value of $1/n$ for Freundlich isotherm (0.174–0.180) shows the high tendency of MO for the adsorption onto MWCNTs, while lower R^2 values (0.902, 0.931 and 0.952) shows

Table 5
Kinetic parameters for the adsorption of MO onto MWCNTs.

Model	Equation	Parameters	Value of parameters	
			19 mg L ⁻¹	40 mg L ⁻¹
First-order kinetic	$\log(q_e - q_t) = \log q_e - \left(\frac{k_1}{2.303}\right)t$	q_e (mg g ⁻¹)	5.860	25.5
		K_1 (g mg ⁻¹ min ⁻¹)	0.430	0.420
		R^2	0.510	0.920
Second-order kinetic	$\frac{t}{q_t} = \frac{1}{k_2 q_e^2} + \frac{t}{q_e}$	q_e (mg g ⁻¹)	123.5	63.30
		K_2 (g mg ⁻¹ min ⁻¹)	0.002	0.030
		R^2	0.999	0.997
Intraparticle diffusion	$q_t = K_{diff} t^{1/2} + C$	C	26.50	37.90
		k_d	3.290	8.560
		R^2	0.881	0.985
Elovich	$q_t = \frac{1}{\beta} \ln(\alpha\beta) + \frac{1}{\beta} \ln t$	α	11.15×10^4	39.68×10^2
		β	0.360	0.140
		R^2	0.870	0.974

Table 6
Comparison for the adsorption of MO onto MWCNTs by different methods and adsorbents.

Adsorbent	Q_{max} (mg g ⁻¹)	Contact time (min)	References
γ -Fe ₂ O ₃ /SiO ₂ /CS composite	34.29	60	[41]
Carbon coated monolith	23.76–47.93	1440	[42]
Multiwalled carbon nanotubes	35.4–64.7	120	[43]
Silkworm exuviae	87.03	720	[44]
Tamarisk-activated carbon	3.84	45	[45]
Mesoporous Fe ₃ O ₄ -SiO ₂ -TiO ₂ (MFST)	2.5	48	[46]
K-d-MnO ₂ nanosheets	145	60	[47]
NH ₂ -MWCNTs	185.53	120	[48]
MWCNTs	53.76	3.4	This work

its unsuitability for fitting the experimental data. The heat of the adsorption and the adsorbent-adsorbate interaction were evaluated by using Temkin isotherm model with known parameters [32]. The lower values of correlation coefficient (0.922, 0.950 and 0.958) correspond to this model show its non-suitability for following experimental data compare to Langmuir model.

3.6. Adsorption kinetic

The determination of adsorption kinetic helps the researchers to predict the rate at which a pollutant is removed from aqueous solutions. This also provides valuable data for understanding the mechanism of sorption reactions and design of industrial adsorption model. The experimental kinetic data of MO adsorption were correlated by pseudo first and second-order, Elovich and intraparticle diffusion model to study the rate and mechanism of adsorption process (Table 5). The experimental adsorption data at initial MO concentration of 19 and 40 mg L⁻¹ using 0.027 g of MWCNT was examined and experimental data are presented in Table 5. In the pseudo-first-order model [33] plotting the values of $\log(q_e - q_t)$ versus t (the equation listed in Table 5) may give a linear relationship. k_1 and q_e values were determined from the slope and intercept, respectively. Distance of intercept from experimental q_e value, indicates that this model was not suitable for fitting the experimental data [34,35]. Hence, the sorption kinetic data were described with the pseudo second-order kinetic equation [36]. In this model, the plot of t/q_t versus t gives a straight line with high correlation coefficient. Constant k_2 and equilibrium adsorption capacity (q_e) were calculated from the intercept and slope of this line, respectively. The high values of R^2 (0.997 and 0.999) strongly confirms the applicability of this model for explanation of adsorption kinetic data (Table 5).

The Elovich equation as another rate equation based on the adsorption capacity in linear form was successfully applied for the adsorption of dye from a aqueous medium [37,38]. The plot of q_t versus $\ln(t)$ should yield a linear relationship with a slope and intercept of $(1/\beta)$ and $(1/\beta) \ln(\alpha\beta)$, respectively. The Elovich constants obtained from the slope and the intercept of the straight line are reported in Table 5. The intraparticle diffusion model relates between adsorption rate and square root of time (t) [39,40]. The values of K_{diff} and C were calculated from the slope and intercept of the plot of q_t versus $t^{1/2}$. C value is related to the thickness of the boundary layer and K_{diff} is the intraparticle diffusion rate constant (mg g⁻¹ min^{-1/2}) were obtained from the final linear portion of above mention plot and presented in Table 5. Since, the intraparticle curve did not pass through the origin; one can notice that in addition to the intraparticle diffusion model another stage such as second order kinetic model control the adsorption process. From Table 5 it is observed that the adsorption of dye followed more closely to pseudo second-order kinetics with regression coefficients >0.99 which fits the experimental data better than the other kinetic models for the entire adsorption process.

3.7. Comparison of the adsorption performance of MWCNTs with other reported adsorbents

A comparison of the results obtained in this study with those in the previously reported works is shown in Table 6 for MO removal using various adsorbents. It may be seen from the table that the dye adsorption capacity of present adsorbent is better than several other adsorbents.

4. Conclusion

In this study, MWCNT coupled with ultrasound assisted adsorption technique was adopted for the removal of MO from aqueous solution. Experiments were designed using RSM and interactions among the various operating parameters were established. It is observed that the MWCNTs having porous structure and high surface area is an efficient adsorbent for the removal of MO from water. It is also concluded that the use of ultrasound led to increase in MO removal percentage in very short time. The optimum operating variables (0.025 g of adsorbent, 3.4 min of contact time and 15 mg L⁻¹ of MO at pH = 1) to achieve maximum removal for adsorption process were determined by CCD. Various standard models were fitted to analyze the adsorption kinetic and equilibrium data. Pseudo second order and Langmuir model was appropriate for analyzing kinetic and isotherm data, respectively. The said adsorbent and the operating conditions considered herein

might of helpful to the design engineers who are going to establish a treatment plant for MO removal.

Acknowledgements

The authors express their appreciation to the Graduate School and Research Council of the University of Yasouj support of this work.

References

- [1] W.-H. Li, Q.-Y. Yue, B.-Y. Gao, Z.-H. Ma, Y.-J. Li, H.-X. Zhao, Preparation and utilization of sludge-based activated carbon for the adsorption of dyes from aqueous solutions, *Chem. Eng. J.* 171 (2011) 320–327.
- [2] Y. Li, Q. Du, T. Liu, Y. Qi, P. Zhang, Z. Wang, Y. Xia, Preparation of activated carbon from *Enteromorpha prolifera* and its use on cationic red X-GRL removal, *Appl. Surf. Sci.* 257 (2011) 10621–10627.
- [3] M. Ghaedi, H. Khajeshari, A. Hemmati Yadkuri, M. Roosta, R. Sahraei, A. Daneshfar, Cadmium hydroxide nanowire loaded on activated carbon as efficient adsorbent for removal of bromocresol green, *Spectrochim. Acta Part A – Mol. Biomol. Spectrosc.* 86 (2012) 62–68.
- [4] M. Kükükosmanoğlu, O. Gezici, A. Ayar, The adsorption behaviors of methylene blue and methyl orange in a diaminoethane sporopollenin-mediated column system, *Sep. Purif. Technol.* 52 (2006) 280–287.
- [5] K.-T. Chung, S.E. Stevens, C.E. Cerniglia, The reduction of azo dyes by the intestinal microflora, *Crit. Rev. Microbiol.* 18 (1992) 175–190.
- [6] K.-T. Chung, The significance of azo-reduction in the mutagenesis and carcinogenesis of azo dyes, *Mutat. Res./Rev. Genet. Toxicol.* 114 (1983) 269–281.
- [7] F. Gulshan, S. Yanagida, Y. Kameshima, T. Isobe, A. Nakajima, K. Okada, Various factors affecting photodecomposition of methylene blue by iron-oxides in an oxalate solution, *Water Res.* 44 (2010) 2876–2884.
- [8] T. Vescovi, H.M. Coleman, R. Amal, The effect of pH on UV-based advanced oxidation technologies–1,4-dioxane degradation, *J. Hazard. Mater.* 182 (2010) 75–79.
- [9] E. Bayram, E. Ayranci, Electrochemically enhanced removal of polycyclic aromatic basic dyes from dilute aqueous solutions by activated carbon cloth electrodes, *Environ. Sci. Technol.* 44 (2010) 6331–6336.
- [10] M.K. Purkait, S. DasGupta, S. De, Resistance in series model for micellar enhanced ultrafiltration of eosin dye, *J. Colloid Interface Sci.* 270 (2004) 496–506.
- [11] I.u. Haq, H.N. Bhatti, M. Asghar, Removal of solar red BA textile dye from aqueous solution by low cost barley husk: equilibrium, kinetic and thermodynamic study, *Can. J. Chem. Eng.* 89 (2011) 593–600.
- [12] B.K. Nandi, A. Goswami, M.K. Purkait, Adsorption characteristics of brilliant green dye on kaolin, *J. Hazard. Mater.* 161 (2009) 387–395.
- [13] B.K. Nandi, A. Goswami, M.K. Purkait, Removal of cationic dyes from aqueous solution by kaolin: kinetic and equilibrium studies, *Appl. Clay Sci.* 42 (2009) 583–590.
- [14] A. Asfaram, M. Ghaedi, S. Hajati, A. Goudarzi, A.A. Bazrafshan, Simultaneous ultrasound-assisted ternary adsorption of dyes onto copper-doped zinc sulfide nanoparticles loaded on activated carbon: optimization by response surface methodology, *Spectrochim. Acta Part A – Mol. Biomol. Spectrosc.* 145 (2015) 203–212.
- [15] M. Roosta, M. Ghaedi, N. Shokri, A. Daneshfar, R. Sahraei, A. Asghari, Optimization of the combined ultrasonic assisted/adsorption method for the removal of malachite green by gold nanoparticles loaded on activated carbon: EXPERIMENTAL design, *Spectrochim. Acta Part A – Mol. Biomol. Spectrosc.* 118 (2014) 55–65.
- [16] A.K. Kumar, S.V. Mohan, Removal of natural and synthetic endocrine disrupting estrogens by multi-walled carbon nanotubes (MWCNT) as adsorbent: kinetic and mechanistic evaluation, *Sep. Purif. Technol.* 87 (2012) 22–30.
- [17] M. Roosta, M. Ghaedi, A. Daneshfar, R. Sahraei, Experimental design based response surface methodology optimization of ultrasonic assisted adsorption of safranin O by tin sulfide nanoparticle loaded on activated carbon, *Spectrochim. Acta Part A – Mol. Biomol. Spectrosc.* 122 (2014) 223–231.
- [18] H.-H. Cho, K. Wepasnick, B.A. Smith, F.K. Bangash, D.H. Fairbrother, W.P. Ball, Sorption of aqueous Zn [II] and Cd [II] by multiwall carbon nanotubes: the relative roles of oxygen-containing functional groups and graphenic carbon, *Langmuir* 26 (2009) 967–981.
- [19] A. Asfaram, M. Ghaedi, S. Hajati, A. Goudarzi, A. Bazrafshan, Simultaneous ultrasound-assisted ternary adsorption of dyes onto copper-doped zinc sulfide nanoparticles loaded on activated carbon: optimization by response surface methodology, *Spectrochim. Acta A 145 (2015) 203–212.*
- [20] B.R. Reddy, T. Sivasankar, M. Sivakumar, V.S. Moholkar, Physical facets of ultrasonic cavitation synthesis of zinc ferrite particles, *Ultrason. Sonochem.* 17 (2010) 416–426.
- [21] M. Roosta, M. Ghaedi, A. Daneshfar, R. Sahraei, A. Asghari, Optimization of the ultrasonic assisted removal of methylene blue by gold nanoparticles loaded on activated carbon using experimental design methodology, *Ultrason. Sonochem.* 21 (2014) 242–252.
- [22] O. Hamdaoui, E. Naffrechoux, Adsorption kinetics of 4-chlorophenol onto granular activated carbon in the presence of high frequency ultrasound, *Ultrason. Sonochem.* 16 (2009) 15–22.
- [23] M. Ghaedi, H. Mazaheri, S. Khodadoust, S. Hajati, M.K. Purkait, Application of central composite design for simultaneous removal of methylene blue and Pb²⁺ ions by walnut wood activated carbon, *Spectrochim. Acta Part A – Mol. Biomol. Spectrosc.* 135 (2015) 479–490.
- [24] M. Ghaedi, S. Hajjati, Z. Mahmudi, I. Tyagi, S. Agarwal, A. Maity, V. Gupta, Modeling of competitive ultrasonic assisted removal of the dyes–methylene blue and safranin-O using Fe₃O₄ nanoparticles, *Chem. Eng. J.* 268 (2015) 28–37.
- [25] S. Khodadoust, M. Ghaedi, R. Sahraei, A. Daneshfar, Application of experimental design for removal of sunset yellow by copper sulfide nanoparticles loaded on activated carbon, *J. Ind. Eng. Chem.* 20 (2014) 2663–2670.
- [26] S. Hajati, M. Ghaedi, H. Mazaheri, Removal of methylene blue from aqueous solution by walnut carbon: optimization using response surface methodology, *Desalination Water Treat.* (2014) 1–15.
- [27] P. Kannusamy, T. Sivalingam, Synthesis of porous chitosan–polyaniline/ZnO hybrid composite and application for removal of reactive orange 16 dye, *Colloids Surf., B* 108 (2013) 229–238.
- [28] I. Langmuir, The constitution and fundamental properties of solids and liquids. Part I solids, *J. Am. Chem. Soc.* 38 (1916) 2221–2295.
- [29] H. Freundlich, Over the adsorption in solution, *J. Phys. Chem.* 57 (1906) 385–470.
- [30] C. Ng, J.N. Lasso, W.E. Marshall, R.M. Rao, Freundlich adsorption isotherms of agricultural by-product-based powdered activated carbons in a geosmin-water system, *Bioresour. Technol.* 85 (2002) 131–135.
- [31] K. Gobi, M. Mashitah, V. Vadivelu, Adsorptive removal of methylene blue using novel adsorbent from palm oil mill effluent waste activated sludge: equilibrium, thermodynamics and kinetic studies, *Chem. Eng. J.* 171 (2011) 1246–1252.
- [32] M. Temkin, V. Pyzhev, Kinetics of ammonia synthesis on promoted iron catalysts, *Acta Physiochim. URSS* 12 (1940) 217–222.
- [33] S. Lagergren, About the theory of so-called adsorption of soluble substances, *Kungliga Svenska Vetenskapsakademiens Handlingar* 24 (1898) 1–39.
- [34] Y. Ho, G. McKay, D.A.J. Wase, C.F. Foster, Study of the sorption of divalent metal ions on to peat, *Adsorpt. Sci. Technol.* 18 (2000) 639–650.
- [35] D. Ruthven, K. Loughlin, The effect of crystallite shape and size distribution on diffusion measurements in molecular sieves, *Chem. Eng. Sci.* 26 (1971) 577–584.
- [36] Y.-S. Ho, G. McKay, Pseudo-second order model for sorption processes, *Process Biochem.* 34 (1999) 451–465.
- [37] E. Bulut, M. Özacar, İ.A. Şengil, Adsorption of malachite green onto bentonite: equilibrium and kinetic studies and process design, *Microporous Mesoporous Mater.* 115 (2008) 234–246.
- [38] S. Chien, W. Clayton, Application of Elovich equation to the kinetics of phosphate release and sorption in soils, *Soil Sci. Soc. Am. J.* 44 (1980) 265–268.
- [39] J.J. Pignatello, F.J. Ferrandino, L.Q. Huang, Elution of aged and freshly added herbicides from a soil, *Environ. Sci. Technol.* 27 (1993) 1563–1571.
- [40] D. Ozdes, C. Duran, H.B. Senturk, Adsorptive removal of Cd (II) and Pb (II) ions from aqueous solutions by using Turkish illitic clay, *J. Environ. Manage.* 92 (2011) 3082–3090.
- [41] H.-Y. Zhu, R. Jiang, L. Xiao, Adsorption of an anionic azo dye by chitosan/kaolin/ γ -Fe₂O₃ composites, *Appl. Clay Sci.* 48 (2010) 522–526.
- [42] S. Hosseini, M.A. Khan, M.R. Malekbala, W. Cheah, T.S. Choong, Carbon coated monolith, a mesoporous material for the removal of methyl orange from aqueous phase: adsorption and desorption studies, *Chem. Eng. J.* 171 (2011) 1124–1131.
- [43] Y. Yao, H. Bing, X. Feifei, C. Xiaofeng, Equilibrium and kinetic studies of methyl orange adsorption on multiwalled carbon nanotubes, *Chem. Eng. J.* 170 (2011) 82–89.
- [44] H. Chen, J. Zhao, J. Wu, G. Dai, Isotherm, thermodynamic, kinetics and adsorption mechanism studies of methyl orange by surfactant modified silkworm exuviae, *J. Hazard. Mater.* 192 (2011) 246–254.
- [45] M. Ghaedi, A.M. Ghaedi, A. Ansari, F. Mohammadi, A. Vafaei, Artificial neural network and particle swarm optimization for removal of methyl orange by gold nanoparticles loaded on activated carbon and *Tamarisk*, *Spectrochim. Acta Part A – Mol. Biomol. Spectrosc.* 132 (2014) 639–654.
- [46] L. Gao, Q. Zhang, J. Li, R. Feng, H. Xu, C. Xue, Adsorption of methyl orange on magnetically separable mesoporous titania nanocomposite, *Chin. J. Chem. Eng.* 22 (2014) 1168–1173.
- [47] Y. Liu, C. Luo, J. Sun, H. Li, Z. Sun, S. Yan, Enhanced adsorption removal of methyl orange from aqueous solution by nanostructured proton-containing δ -MnO₂, *J. Mater. Chem. A* 3 (2015) 5674–5682.
- [48] Y. Liu, G. Cui, C. Luo, L. Zhang, Y. Guo, S. Yan, Synthesis, characterization and application of amino-functionalized multi-walled carbon nanotubes for effective fast removal of methyl orange from aqueous solution, *RSC Adv.* 4 (2014) 55162–55172.